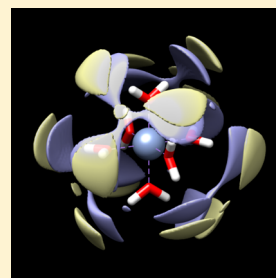


Three-Dimensional Reference Interaction Site Model Self-Consistent Field Study of the Electronic Structure of $[\text{Cr}(\text{H}_2\text{O})_6]^{3+}$ in Aqueous Solution

Shinya Fujishige, Yukio Kawashima,[†] Norio Yoshida,^{*} and Haruyuki Nakano^{*}

Department of Chemistry, Graduate School of Sciences, Kyushu University, Fukuoka 812-8581, Japan

ABSTRACT: The three-dimensional reference interaction-site model self-consistent-field (3D-RISM-SCF) method was applied to the electronic structure of hexahydrated chromium trication $[\text{Cr}(\text{H}_2\text{O})_6]^{3+}$ in aqueous solution. The 3D distribution around $[\text{Cr}(\text{H}_2\text{O})_6]^{3+}$ showed 12 maximum density points arising from hydrogen bonds, as well as eight local maximum points at the hollow sites, in the second hydration shell. The 3D distribution function also indicated 20 local maximum sites in the third hydration shell. The low-lying excited states of vertical transitions were computed using time-dependent density functional theory (TD-DFT), including the electric field from the solvent. The electronic configurations and excitation energies calculated using DFT and 3D-RISM-SCF were very similar, although the orbital energies involved in the transition were rather different. The two lowest excited states (1^4T and 2^4T) were roughly assigned to the d–d transitions, and the third and fourth excited states (3^4T and 4^4T) were assigned to ligand-to-metal charge-transfer transitions. The computed excited energies were in good agreement with the experimental values.



I. INTRODUCTION

Hydration of transition metals plays an important role in condensed-phase chemistry and biochemistry. Therefore, hydrated metal ions have been the subject of extensive experimental and theoretical studies. For instance, to investigate the static structure of hydrated ions, a variety of experimental techniques, such as X-ray and neutron diffraction experiments, have been applied. Theoretical approaches also have been applied because of the development of electronic structure theory and solution theory based on simulation. In particular, the excited state electronic structures as well as the ground state have been well elucidated recently using density functional theory (DFT) or multiconfigurational electronic structure theory.

The properties of complexes of transition metal ions are influenced by the large variation in the d-electron configurations. In solution, the changes in geometrical structure, chemical reactions, and thermodynamic properties of the complexes along the series show similar trends for different ligands. In aqueous solution, the first-row transition metal dications and trications are surrounded by an inner hydration shell of six water molecules, resulting in an octahedral or near-octahedral species. Crystal field theory states that the resulting field splits the degenerate atomic 3d orbitals into molecular e_g and t_{2g} orbitals. The traditional view is that the characteristic absorption bands in the visible and near-ultraviolet regions are due to transitions between these molecular orbitals (MO).

Many theoretical studies have been conducted so far. The simplest way to model the hydrated ions is treating an essential part of them as an isolated quantum system. Aakesson and co-workers¹ obtained binding energies and metal–oxygen (M–O) bond distances using Hartree–Fock calculations for the divalent and trivalent metal ions of the first-row transition

metals. They found that the variation of the calculated M–O bond distances was consistent with the trend expected from ligand-field theory. Landry-Hum and co-workers² studied triplet electronic states in d^2 and d^8 complexes ($[\text{V}(\text{H}_2\text{O})_6]^{3+}$ and $[\text{Ni}(\text{H}_2\text{O})_6]^{2+}$, respectively) using absorption spectroscopy and high level ab initio molecular orbital analysis. They used the complete active space self-consistent field method followed by second-order perturbation theory (CAS-SCF/CASPT2) and found that octahedral complexes of transition metal ions with d^2 and d^8 electron configurations have triplet electronic states with identical T_{2g} , A_{2g} , $T_{1g}(^3F)$, and $T_{1g}(^3P)$ symmetry labels. However, these theoretical calculations did not include the solvent effects from beyond the ligand molecules.

To include the solvent effects, Chillemi and co-workers³ have developed an effective computational procedure for the structural and dynamical investigation of ions. In their methods, quantum mechanical energy surfaces for the interaction of a transition metal ion with a water molecule have been calculated taking into account the effect of bulk solvent using the polarizable continuum model (PCM). The effective ion–water interactions were fitted using suitable analytical potentials and have been utilized in molecular dynamics simulations to obtain structural and dynamical properties of ionic aqueous solutions. A combined ab initio quantum mechanics/molecular mechanical (QM/MM) approach was developed by Rode and co-workers.⁴ They treated the ion and its first hydration sphere at the Born–Oppenheimer ab initio quantum mechanical level, while classical pair and three-body potentials were employed for the rest of the system. Iuchi and co-workers⁵ constructed a

Received: June 14, 2013

Revised: August 5, 2013

Published: August 16, 2013

model Hamiltonian to describe the electronic structure of Ni^{2+} in aqueous solution using multiconfigurational quasidegenerate perturbation theory (MC-QDPT). Using the model Hamiltonian, they performed molecular dynamics simulation calculations for the ground state of Ni^{2+} in aqueous solution to calculate the electronic absorption spectral shape as well as the ground state properties. Although these theoretical methods successfully account for solvation structures and properties of transition metal ions, it is not a simple task to describe the electronic excitation of a transition metal ion in solution quantitatively even now.

A difficulty in studying excited states is that most of the dications and trications of the 3d transition metal hexahydrates have degenerate ground states because of their high molecular symmetry. In such a situation, state averaging (or configuration averaging) is necessary to treat the degenerate ground states equally, avoiding nonequivalent degenerate MOs or states, which limits the electronic structure studies on the transition metal complexes. The state-averaging multiconfigurational self-consistent field (SA-MCSCF) method is a solution to this problem. However, the SA-MCSCF results are not so quantitative, especially for excited states, and therefore, subsequent use of costly multireference perturbation or configuration-interaction methods is necessary to obtain accurate results.

In the present article, we examine the electronic structure of chromium hexahydrate trication $[\text{Cr}(\text{H}_2\text{O})_6]^{3+}$ and its solvation structure in aqueous solution in detail as an example of transition metal ions in solution, using DFT and time-dependent DFT (TD-DFT) coupled with the three-dimensional reference interaction-site model (3D-RISM-SCF/DFT)^{6,7} as well as the one-dimensional version of RISM-SCF/DFT.⁸ The 3D-RISM-SCF method is a hybrid method of ab initio electronic structure theory and the integral equation theory for solutions. The trication $[\text{Cr}(\text{H}_2\text{O})_6]^{3+}$ has a nondegenerate ground state; namely, it is an exception to the degenerate ground state complexes, along with $[\text{Co}(\text{H}_2\text{O})_6]^{3+}$. Thus, some advantages of DFT, such as computational compactness and variationality, are fully utilized during the SCF process between electronic and solution states in the 3D-RISM-SCF calculation.

The organization of this article is as follows. In section II, we describe the computational method and the details of the calculations used in the present article. Section III shows the results of the calculations. The optimized structure of $[\text{Cr}(\text{H}_2\text{O})_6]^{3+}$, the solvation structure, the ground and excited state electronic structures, and vertical excitation energies are reported and discussed. Conclusions are given in section IV.

II. COMPUTATIONAL METHODS

Brief Overview of the 3D-RISM-SCF Method. We very briefly review the 3D-RISM-SCF method. The 3D-RISM-SCF method^{6,7} is a combined method of electronic structure theory and integral equation theory, which is an extension of the RISM-SCF method (in this article, called the 1D-RISM-SCF method)⁸ initially developed by Ten-no, Hirata, and Kato. The solvated molecule is treated by quantum chemistry, whereas the surrounding solvent molecules are treated by statistical mechanics.

Assume a molecule in solution at infinite dilution. The Helmholtz free energy A of the solute–solvent system is given as the sum

$$A = E_{\text{solute}} + \Delta\mu \quad (1)$$

where E_{solute} is the solute electronic energy computed from quantum chemical electronic structure theory and $\Delta\mu$ is the excess chemical potential coming from the solute–solvent interaction. In the 3D-RISM-SCF method, the excess chemical potential is computed from the number density of the solvent ρ_v and the interaction potential between the solute molecule and solvent site γ at point \mathbf{r} :

$$\Delta\mu = \rho_v \int_0^1 d\lambda \int d\mathbf{r} \sum_{\gamma \in \text{solvent}} \lambda u_\gamma(\mathbf{r}) g_\gamma^\lambda(\mathbf{r}) \quad (2)$$

where $g_\gamma^\lambda(\mathbf{r})$ and $u_\gamma(\mathbf{r})$ denote the 3D distribution function and solute–solvent interaction potential, respectively. If we employ Kovalenko–Hirata (KH) closure,^{6,9} this equation becomes

$$\Delta\mu = \rho_v k_B T \sum_{\gamma \in \text{solvent}} \int d\mathbf{r} [(h_\gamma(\mathbf{r}))^2 \theta(-h_\gamma(\mathbf{r}))/2 - c_\gamma(\mathbf{r}) - h_\gamma(\mathbf{r})c_\gamma(\mathbf{r})/2] \quad (3)$$

Here, k_B is the Boltzmann constant, T is the absolute temperature, and $\theta(x)$ is the Heaviside step function. Functions $h_\gamma(\mathbf{r})$ and $c_\gamma(\mathbf{r})$ are the 3D-site total and direct correlation functions, respectively.

The Helmholtz free energy is a functional of the electronic wave function Ψ (or electronic density in DFT) of the solute molecule, and the correlation functions $h_\gamma(\mathbf{r})$ and $c_\gamma(\mathbf{r})$: $A = A[\Psi, h_\gamma(\mathbf{r}), c_\gamma(\mathbf{r})]$. The basic equations of the 3D-RISM-SCF method are derived by the variation of the free energy, eq 1, with respect to the electronic wave function (or the electronic density in DFT) and the correlation functions, $h_\gamma(\mathbf{r})$ and $c_\gamma(\mathbf{r})$.^{6,7} If we adopt Kohn–Sham DFT for the solute electronic structure theory, the resulting equation for the solute molecules is the Kohn–Sham equation (KS) for the KS operator f that includes the interaction from the solvent molecules:

$$f\varphi(\mathbf{r}) = \varepsilon\varphi(\mathbf{r}) \quad (4)$$

where ε and $\varphi(\mathbf{r})$ are the orbital energy and KS orbital, respectively. The equations for the solvent are the KH closure relation and the 3D-site Ornstein–Zernike (OZ) equation:^{9,10}

$$h_\gamma(\mathbf{r}) = c_\gamma(\mathbf{r}) * (\omega_{l_\gamma}(r) + \rho_v h_{l_\gamma}^{vv}(r)) \quad (5)$$

where $\omega_{l_\gamma}(r) = \delta(r - l_\gamma)$ is the intramolecular correlation matrix of a solvent molecule with site separation l_γ , and the operation symbol $*$ means the convolution in direct space and summation over repeated site indices. This matrix ω_{l_γ} describes the molecular structure of solvents in the interaction site model by giving distance constraints to all pairs of atoms. These basic eqs 4 and 5 (with the KH closure relation) are coupled with each other via the interaction potentials between the solute and solvent molecules, and supplemented by the solvent–solvent 1D-RISM equation:¹¹

$$\mathbf{h}^{vv}(r) = \boldsymbol{\omega}(r) * \mathbf{c}^{vv}(r) * (\boldsymbol{\omega}(r) + \rho_v \mathbf{h}^{vv}(r)) \quad (6)$$

where the superscript vv denotes solvent–solvent functions and the matrix elements of \mathbf{h}^{vv} , $\boldsymbol{\omega}$, and \mathbf{c}^{vv} are $h_{l_\gamma}^{vv}$, ω_{l_γ} , and $c_{l_\gamma}^{vv}$, respectively. In the 1D-RISM-SCF method, eqs 2, 3, and 5 are replaced by the equations

$$\Delta\mu = 4\pi\rho_v \int_0^1 d\lambda \int d\mathbf{r} \sum_{\alpha \in \text{solute}} \sum_{\gamma \in \text{solvent}} \lambda u_{\alpha\gamma}(\mathbf{r}) g_{\alpha\gamma}^\lambda(\mathbf{r}) r^2 \quad (7)$$

$$\Delta\mu = 4\pi\rho_{\nu}k_{\text{B}}T \sum_{\alpha \in \text{solute}} \sum_{\gamma \in \text{solvent}} \int dr r^2 [(h_{\alpha\gamma}(r))^2 \theta(-h_{\alpha\gamma}(r))] / 2 - c_{\alpha\gamma}(r) - h_{\alpha\gamma}(r)c_{\alpha\gamma}(r)/2 \quad (8)$$

$$\mathbf{h}(r) = \boldsymbol{\omega}(r) * \mathbf{c}(r) * (\boldsymbol{\omega}(r) + \rho_{\nu} \mathbf{h}(r)) \quad (9)$$

respectively. It is noted that the intramolecular correlation matrix, $\omega_{\nu}(r)$, appears twice in the 1D-RISM equation, eqs 6 and 9, while only once in the 3D-RISM equation, eq 5. This is because the 1D-RISM employs the interaction site model for both the solute and solvent, whereas 3D-RISM employs only for the solvent. Using these equations, the electronic structure of the solute molecules and solvent structure are determined self-consistently. The derivation and applications of the 3D- and 1D-RISM-SCF methods have been described previously.^{6–8,12}

Computational Details. The geometry of $[\text{Cr}(\text{H}_2\text{O})_6]^{3+}$, the ground electronic structures, and the solvent distribution around the ion were determined by the 3D- and 1D-RISM-SCF methods described in the previous subsection. The excited states were obtained using TD-DFT. (Gas phase calculations were also done for comparison with those in the solution phase.) The electronic structure method for the solute molecules used in the 3D- and 1D-RISM-SCF method was DFT with the Becke three-parameter, Lee–Yang–Parr (B3LYP) exchange–correlation functional.¹³ The basis set used was the correlation-consistent polarized valence triple- ζ (cc-pVTZ) set.¹⁴ The relativistic effect was included with the infinite-order two-component one-electron Hamiltonian developed by Barysz and co-workers.¹⁵

The parameters used in the 3D- and 1D-RISM-SCF methods were as follows. The temperature and the density of solvent water were 298 K and 0.03334 molecules per \AA^3 , respectively. Effective point charges were employed to describe the solute–solvent interaction potential. The effective point charges on the solute molecule were determined to reproduce the electrostatic potential around the solute molecule by using least-squares fitting. The Lennard–Jones (LJ) parameters (σ , ϵ) for Cr, H, and O were (2.2 \AA , 0.0125 kcal/mol), (0.4 \AA , 0.046 kcal/mol), and (3.166 \AA , 0.1554 kcal/mol), respectively. The extended simple point charge model (SPC/E) parameter set for the geometrical and potential parameters for the solvent water was employed with modified hydrogen parameters ($\sigma = 0.4 \text{\AA}$ and $\epsilon = 0.046 \text{ kcal/mol}$).¹⁶ No LJ parameters for Cr suitable to our calculations have been reported to our knowledge. Therefore, those for Zn taken from Amber 99 parameter set were employed.¹⁷ Since the Cr ion is surrounded by the coordination waters in the present model, the LJ interaction between the Cr ion and the solvent waters can be assumed to be small. The influence of using the Zn parameter set should have only limited effects in the results. The grid points in the 3D-RISM calculations were $256 \times 256 \times 256$ with a spacing of 0.1 \AA , and those in the 1D-RISM-SCF calculations were 2048 with a spacing of 0.01 \AA .

All of the calculations were performed with a modified version of the GAMESS program package,¹⁸ where the 3D- and 1D-RISM-SCF and their gradient methods have been implemented.¹⁰

In the following sections, we will refer to the gas phase DFT, 3D-RISM-SCF/DFT, and 1D-RISM-SCF/DFT methods simply as the (gas phase) DFT, 3D-RISM-SCF, and 1D-RISM-SCF methods, respectively, as a shorthand notation.

III. RESULTS AND DISCUSSION

Molecular Structure of the Solute. The calculated geometrical parameters of the $[\text{Cr}(\text{H}_2\text{O})_6]^{3+}$ ion obtained using the DFT, 3D-RISM-SCF, and 1D-RISM-SCF methods are summarized in Table 1. The optimized structure has T_h

Table 1. Geometrical Parameters of $[\text{Cr}(\text{H}_2\text{O})_6]^{3+}$ (Distances in \AA and Angles in Degrees)

	gas	solution	
		3D-RISM-SCF	1D-RISM-SCF
$r(\text{Cr–O})$	2.007	2.010	1.973
$r(\text{O–H})$	0.974	0.977	0.979
$\angle\text{HOH}$	107.9	110.1	110.2
torsion angle ^a	0.0	6.5	17.8
symmetry	T_h	T	T

^aTorsion angles indicate the dihedral angle between the CrO_4 and H_2O planes.

symmetry in the gas phase, while that in the solution phase is almost T_h symmetry but slightly distorted, taking T symmetry. The difference is the ligand water orientation: distorted by 6.5 and 17.8 degrees for 3D-RISM-SCF and 1D-RISM-SCF calculations, respectively. The bond distances for the gas (2.007 \AA) and 3D-RISM-SCF (2.010 \AA) calculations are very close to each other. In contrast, the distance obtained from the 1D-RISM-SCF method, 1.973 \AA , is somewhat smaller. This is attributed to a general feature of the 3D- and 1D-RISM-SCF methods: the 1D-RISM-SCF method tends to overestimate the electrostatic interaction compared with the 3D-RISM-SCF method. Table 2 shows the Mulliken charges of the atoms in $[\text{Cr}(\text{H}_2\text{O})_6]^{3+}$ in the gas and solution phases. The feature is illustrated by the charge on the Cr and O atoms. The 1D-RISM-SCF charges, 1.229 on Cr and -0.438 on O, are larger in absolute value than the 3D-RISM-SCF charges of 1.186 and -0.375 , respectively. This larger polarization of Cr–O bonds is responsible for the shorter bond distance in the 1D-RISM-SCF method. Note that the larger polarization of the 1D-RISM-SCF method did not change even if it was computed at the 3D-RISM-SCF geometry. The gas phase and 3D-RISM-SCF results for the molecular structure are in good agreement with previous experimental and computational results.¹⁸

Solvation Structure. Figure 1 shows the three-dimensional distribution of oxygen and hydrogen atoms of the solvent molecules obtained with the 3D-RISM-SCF calculations. There are 12 highest density points in the direction of O to H of the ligand H_2O (Figure 1a). The distances of the solvent oxygen and solvent hydrogen highest points from the hydrogen of the ligand are 1.6 and 2.4 \AA , respectively. These data clearly show the hydrogen bonds between the ligands and solvent H_2O molecules in the second shell. In addition, there are also high density points in the eight hollow sites among three ligand H_2Os .

From the analysis of the 3D distribution function, the highest density points of oxygen and hydrogen are at (0.2, 2.3, and 3.2 \AA) [3.9 \AA from Cr] and (0.2, 3.0, and 3.6 \AA) [4.7 \AA from Cr], respectively, and their equivalent points. Here, the coordinate system has been taken to set the origin at the Cr atom and the x -, y -, and z -axes along the Cr–O bond directions. The highest densities are 8.1 for oxygen and 2.5 for hydrogen. Note that these values include about 0.1 \AA distance and 0.1 density errors originating from the 0.1 \AA unit 3D grids in the 3D-RISM

Table 2. Mulliken Charges

atom	gas	solution		gas ^a	solution
		3D-RISM-SCF	1D-RISM-SCF		1D-RISM-SCF ^b
Cr	1.162	1.186	1.229	1.158	1.203
O	-0.354	-0.375	-0.438	-0.359	-0.427
H	0.330	0.339	0.367	0.333	0.363

^aGas phase DFT charges at the 3D-RISM-SCF geometry. ^b1D-RISM-SCF charges at the 3D-RISM-SCF geometry.

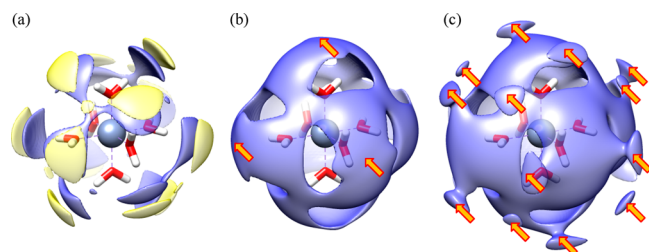


Figure 1. (a) Distribution of oxygen (light blue; 4.0) and hydrogen (light yellow; 2.0) of water molecules around the $[\text{Cr}(\text{H}_2\text{O})_2]^{3+}$ ion; (b) overlap region corresponding to the shoulder on the initial peak of the angular averaged radial distribution function of oxygen (isovalue, 1.75) [3 out of total 6 sites are pointed by the arrows]; and (c) 3D distribution corresponding to the second peak (the third shell) of the angular averaged radial distribution function of oxygen (isovalue, 1.35) [13 out of total 20 sites are pointed by the arrows].

method. The local maxima of the density in the eight hollow sites are at (2.0, 2.0, and 2.0 Å) [3.5 Å from Cr] for oxygen and at (2.5, 2.5, and 2.5 Å) [4.3 Å from Cr] for hydrogen and their seven equivalent points for each. However, the density at the local maxima is relatively small compared with that at the highest points. The density values at these points are 4.9 for oxygen and 2.1 for hydrogen. These local maxima are simply due to the space available that is not excluded by the ligand H_2O . The 3D distribution function also indicates 20 local maximum sites in the third hydration shell (Figure 1c).

Figure 2a shows the radial distribution functions of oxygen and hydrogen from Cr obtained by angular averaging of the 3D distribution function, as well as the coordination number of oxygen atoms. The maxima of the radial distribution functions are given at 4.1 and 4.9 Å for O and H, respectively [maximum

values, 1.5 (O) and 1.3 (H)]. These maxima clearly correspond to the density maxima of the 3D distribution functions. In contrast, there are no peaks that correspond to the local maxima at the hollow sites for the 3D distribution function. This indicates that the local maxima are rather isolated and small.

A small shoulder associated with the largest peak of O is found at about 4.5 Å. This was identified from the 3D distribution function analysis as the shoulder arising from the overlap between the two adjacent maxima (Figure 1b). The second peak in Figure 2a corresponds to the 20 local maximum sites in the third hydration shell shown in Figure 1c.

Figure 2b also shows radial distribution functions but for a hydrogen atom of the ligand H_2O . Three peaks that show the solvent structure are found in the $g_{\text{H-O}}(r)$ function. The leftmost peak at 1.8 Å corresponds to the 3D maxima and clearly shows the existence of hydrogen bonds between ligand and solvent in the second shell.

The 1D-RISM-SCF results are summarized in Figure 3. This figure correspond to Figure 2 of the 3D-RISM-SCF calculations. There are apparent differences in the heights and widths of the peaks, although the peak positions are close to each other. The RISM-SCF peaks are narrow and high compared with the 3D-RISM-SCF peaks. This feature is especially notable for the leftmost peak of the $g_{\text{H-O}}(r)$ in Figure 3b.

The radial distribution functions of $[\text{Cr}(\text{H}_2\text{O})_6]^{3+}$ have also been reported by Bleuzen and co-workers¹⁹ and Pappalardo and co-workers.²⁰ Bleuzen and co-workers performed molecular dynamics simulations as well as ¹⁷O nuclear magnetic resonance measurements; however, Pappalardo and co-workers performed Monte Carlo simulations. They both obtained

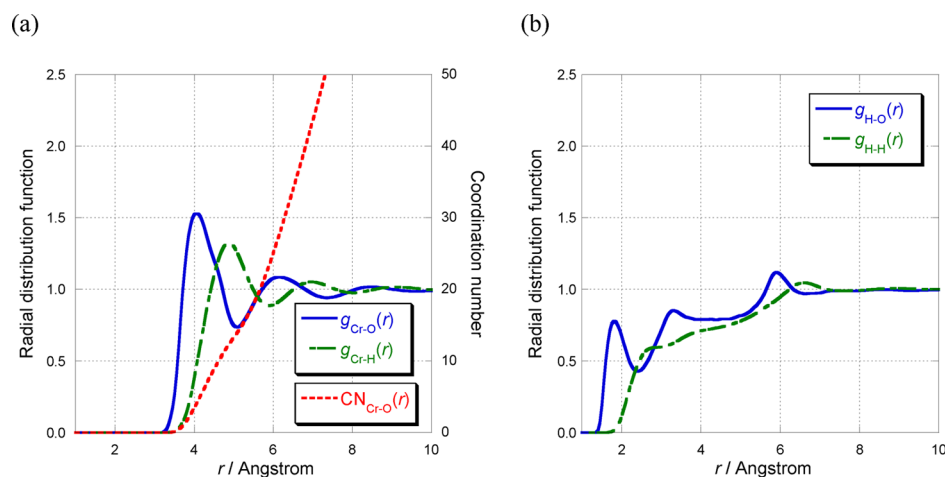


Figure 2. (a) Radial distribution functions of oxygen and hydrogen from Cr obtained by angular averaging of the 3D distribution function and the coordination number (CN) of the oxygen atoms; (b) radial distribution functions of oxygen and hydrogen from a H atom of the ligand H_2O obtained by angular averaging.

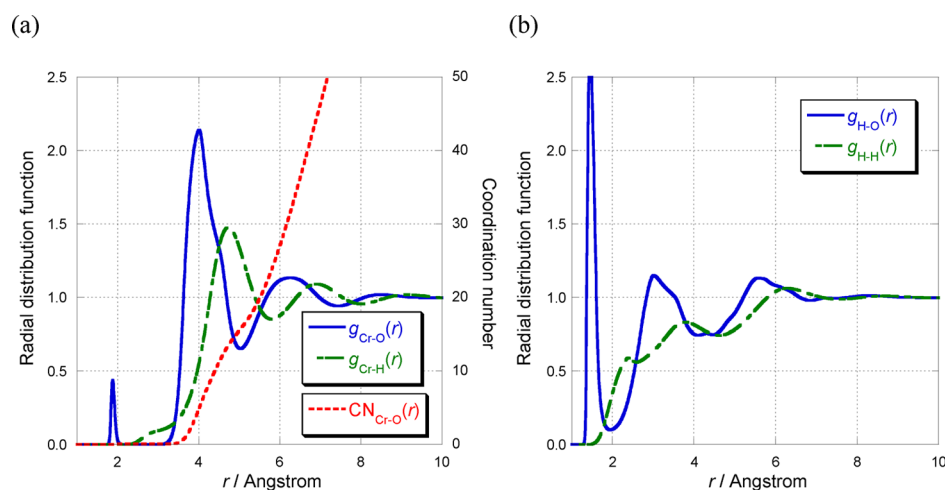


Figure 3. (a) Radial distribution functions of oxygen and hydrogen from Cr obtained using the 1D-RISM-SCF method and the coordination number of the oxygen atoms; (b) radial distribution functions of oxygen and hydrogen from a H atom of the ligand H₂O obtained using the 1D-RISM-SCF method.

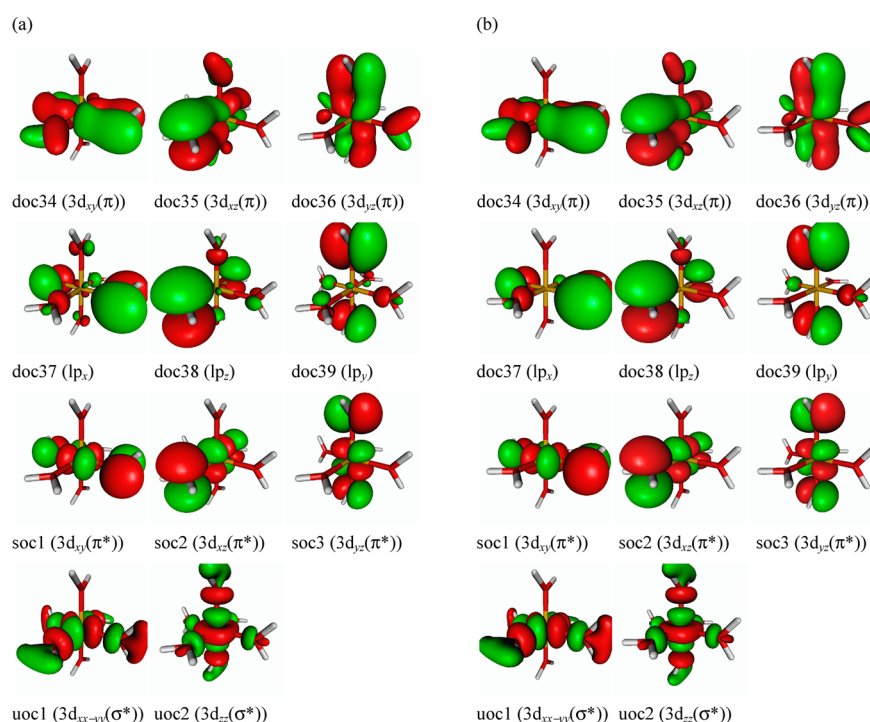


Figure 4. Molecular orbitals involved in the d–d and ligand-to-metal excited states of [Cr(H₂O)₆]³⁺ in (a) aqueous solution and (b) the gas phase. The labels docX, socY, and uocZ stand for the Xth doubly occupied, Yth singly occupied, and Zth unoccupied orbitals, respectively.

similar radial distribution functions and coordination numbers. Their peaks are in very good agreement with ours in position, while they are higher and narrower than the present 1D-RISM-SCF results.

We finally note that the small peak in the $g_{\text{Cr-O}}(r)$ at about 1.9 Å in Figure 3a is an artifact, which probably arose from the underestimation of the steric hindrance effects between the oxygen of a solvent water and a coordination water.

Electronic Structures of the Ground and Low-Lying Excited States. Figure 4 shows some selected alpha MOs obtained from the 3D-RISM-SCF and DFT methods. Only MOs involved in the transitions of the four (triply degenerate) low-lying excited states are shown. The MO set obtained with

the 1D-RISM-SCF method is not shown because they are very similar to those with the 3D-RISM-SCF method.

The first three MOs are triply degenerate (t or t_g in the T or T_h symmetry cases, respectively) π bonding orbitals composed of Cr 3d (d_{xz} , d_{yz} , and d_{xy}) and H₂O lone pair (lp) orbitals. The seventh–ninth and 10–11th MOs are triply (t or t_g) and doubly (e or e_g) degenerate π and σ antibonding orbitals, respectively, with the same components as the first–third MOs (d_{xy} , d_{xz} , and d_{yz} for t (t_g) and d_{xx-yy} and $d_{zz-(xx+yy)/2}$ for e (e_g)). In contrast, the fourth–sixth MOs are degenerate t (t_u) orbitals composed of H₂O lp orbitals. Hereafter, these MOs are denoted $3d_{xy}(\pi)$, $3d_{xz}(\pi)$, $3d_{yz}(\pi)$, $3d_{xy}(\pi^*)$, $3d_{xz}(\pi^*)$, $3d_{yz}(\pi^*)$, $3d_{xx-yy}(\sigma^*)$, $3d_{zz}(\sigma^*)$, lp_x , lp_y , and lp_z as a shorthand notation. The shapes of the MOs in the solution and gas phases

Table 3. Excitation Energies and Configurations

state	configuration	gas	solution		
			3D-RISM-SCF	1D-RISM-SCF	1D-RISM-SCF ^a
		2.21 eV	2.20 eV	2.43 eV	2.24 eV
1 ⁴ T (1 ⁴ T _g)	3d _{xy} (π*) → 3d _{xx-yy} (σ*)	0.918	0.921	0.949	0.926
	3d _{xy} (π) → 3d _{xx-yy} (σ*)	0.396	0.386	0.296	0.373
1 ⁴ T'	3d _{xz} (π*) → 3d _{zz} (σ*)	0.788	0.791	0.817	0.796
	3d _{xz} (π) → 3d _{zz} (σ*)	-0.471	-0.472	-0.483	-0.474
	3d _{xz} (π) → 3d _{zz} (σ*)	0.344	0.335	0.257	0.324
1 ⁴ T''	3d _{yz} (π*) → 3d _{zz} (σ*)	0.802	0.804	0.827	0.809
	3d _{yz} (π*) → 3d _{xx-yy} (σ*)	0.447	0.449	0.466	0.452
	3d _{yz} (π) → 3d _{zz} (σ*)	-0.342	-0.333	-0.256	-0.322
		2.85 eV	2.86 eV	3.07 eV	2.89 eV
2 ⁴ T (2 ⁴ T _g)	3d _{xy} (π*) → 3d _{zz} (σ*)	0.933	0.935	0.958	0.939
	3d _{xy} (π) → 3d _{zz} (σ*)	0.350	0.341	0.261	0.330
2 ⁴ T'	3d _{xz} (π*) → 3d _{xx-yy} (σ*)	0.805	0.806	0.826	0.810
	3d _{xz} (π) → 3d _{zz} (σ*)	0.473	0.474	0.484	0.476
	3d _{xz} (π) → 3d _{xx-yy} (σ*)	0.296	0.289	0.222	0.280
2 ⁴ T''	3d _{yz} (π*) → 3d _{xx-yy} (σ*)	0.812	0.814	0.832	0.817
	3d _{yz} (π*) → 3d _{zz} (σ*)	-0.460	-0.461	-0.473	-0.463
	3d _{yz} (π) → 3d _{xx-yy} (σ*)	-0.309	-0.302	-0.230	-0.292
		5.60 eV	5.62 eV	6.11 eV	5.72 eV
3 ⁴ T (3 ⁴ T _g)	lp _y → 3d _{zz} (σ*)	0.994	0.987	0.959	0.987
3 ⁴ T'	lp _x → 3d _{xx-yy} (σ*)	0.862	0.837	0.733	0.836
	lp _x → 3d _{zz} (σ*)	0.494	0.525	0.649	0.527
3 ⁴ T''	lp _z → 3d _{xx-yy} (σ*)	0.859	0.873	0.929	0.874
	lp _z → 3d _{zz} (σ*)	-0.499	-0.462	-0.310	-0.460
		5.81 eV	5.80 eV	6.24 eV	5.90 eV
4 ⁴ T (4 ⁴ T _g)	lp _y → 3d _{xx-yy} (σ*)	0.987	0.929	0.907	0.925
	3d _{xz} (π) → 3d _{xx-yy} (σ*)		-0.266		-0.275
	lp _x → 3d _{xy} (σ*) (β) ^b			-0.264	
4 ⁴ T'	lp _x → 3d _{zz} (σ*)	0.861	0.777	0.686	0.771
	lp _x → 3d _{xx-yy} (σ*)	-0.483	-0.514	-0.626	-0.514
	3d _{yz} (π) → 3d _{zz} (σ*)		0.293	0.206	0.304
4 ⁴ T''	lp _z → 3d _{xz} (π*) (β) ^b			-0.264	
	lp _z → 3d _{zz} (σ*)	0.849	0.833	0.885	0.831
	lp _z → 3d _{xx-yy} (σ*)	0.504	0.416	0.281	0.411
	3d _{xy} (π) → 3d _{xx-yy} (σ*)		-0.242		-0.251
				0.264	

^a1D-RISM-SCF results at the 3D-RISM-SCF geometry. ^bThe symbol (β) indicates the beta spin transition.

are very similar to each other. However, there are some differences because of the differences of molecular symmetry. For instance, lp_x, lp_y, and lp_z in the solution phase have small contributions from Cr 3d orbitals, while those in the gas phase do not.

Although the shapes are similar in the gas and solution phases, the orbital energies are quite different because of the electric field from the solvent water in the second and outer shells in the present model. The orbital energies of the MOs shown in Figure 4 were -24.60, -23.70, -22.46, and -16.62 eV in the gas phase, which were destabilized to -17.08, -16.17, -14.93, and -9.05 eV (3D-RISM-SCF) and -13.19, -12.17, -10.74, and -4.55 eV (1D-RISM-SCF) in the solution phase. Because these differences are not ascribed to the shapes of the MOs, this fact indicates that the 1D-RISM electric field is stronger than the 3D-RISM electric field. An interesting feature is that the orbital energy splittings are very similar in the gas and 3D-RISM solution phases, while they are somewhat

different from the 1D-RISM solution phase. This affects the orbital picture of the transition to some excited states, as seen below.

Table 3 summarizes the vertical excitation energies and orbital characters for the four low-lying excited states computed for the gas and solution phases. The absorption spectra of aqueous solutions of Cr³⁺ ion show bands at 17 000 and 24 000 cm⁻¹.²¹ The assignment of these bands is the transition from the ⁴A_{2g} ground state to excited quartet states, namely,

$${}^4T_{2g}(\text{F}) \leftarrow {}^4A_{2g}(\text{F}) \quad 17000 \text{ cm}^{-1} (2.11 \text{ eV})$$

$${}^4T_{1g}(\text{F}) \leftarrow {}^4A_{2g}(\text{F}) \quad 24000 \text{ cm}^{-1} (2.98 \text{ eV})$$

where the state terms are written in the O_h point group symmetry terminology.

The first and second states (1⁴T and 2⁴T) are both triply degenerate states composed of the configurations from the

antibonding occupied orbital group ($3d_{xy}(\pi^*)$, $3d_{xz}(\pi^*)$, and $3d_{yz}(\pi^*)$) to the antibonding virtual orbital group ($3d_{xx-yy}(\sigma^*)$ and $3d_{zz}(\sigma^*)$). The excitation energy to the first excited state was computed to be 2.21, 2.20, and 2.43 eV by the DFT, 3D-RISM-SCF, and 1D-RISM-SCF methods. (These correspond to the 17 000 cm^{-1} band in the experiment.) The DFT and 3D-RISM-SCF excitation energies are in good agreement with the experimental 17 000 cm^{-1} (2.11 eV). However, the 1D-RISM-SCF method overestimates it by 0.32 eV. An orbital picture of a substate of the 1^4T (or 1^4T_g) state was the $3d_{xy}(\pi^*)$ to $3d_{xx-yy}(\sigma^*)$ transition with a small contribution from the $3d_{xy}(\pi)$ to $3d_{xx-yy}(\sigma^*)$ transition. Because the positive phase of the mixing of $3d_{xy}(\pi^*)$ and $3d_{xy}(\pi)$ means the enhancement of d_{xy} and reduction of lp contribution, this state can be roughly interpreted as a d–d transition. The other two degenerate substates ($1^4T'$ and $1^4T''$) look like linear combinations of the $3d(\pi^*)$ to $3d_{zz}(\sigma^*)$ and the $3d(\pi^*)$ to $3d_{xx-yy}(\sigma^*)$ transitions. However, these can be rewritten as $3d_{xz}(\pi^*)$ to $3d_{xx-zz}(\sigma^*)$ and $3d_{yz}(\pi^*)$ to $3d_{yy-zz}(\sigma^*)$ if we use a redundant nonorthogonal MO set $\{3d_{xx-yy}(\sigma^*), 3d_{xx-zz}(\sigma^*), \text{ and } 3d_{yy-zz}(\sigma^*)\}$ made from $\{3d_{zz}(\sigma^*) \text{ and } 3d_{xx-yy}(\sigma^*)\}$. Here, we have used the relationships that the 3d atomic orbitals satisfy:

$$2d_{zz-(xx+yy)}/2 - d_{xx-yy} = -2d_{xx-zz} \quad (10)$$

$$2d_{zz-(xx+yy)}/2 + d_{xx-yy} = -2d_{yy-zz} \quad (11)$$

The excitation energy to the 2^4T state was computed to be 2.85, 2.86, and 3.07 eV by the DFT, 3D-RISM-SCF, and 1D-RISM-SCF methods, respectively. These correspond to the 24 000 cm^{-1} (2.98 eV) band of the absorption spectra. The computed values were close to the experimental values, although the DFT and 3D-RISM-SCF methods slightly underestimated and the 1D-RISM-SCF method slightly overestimated the values. The initial substate of the 2^4T (or 2^4T_g) state is mainly due to the $3d_{xy}(\pi^*)$ to $3d_{zz}(\sigma^*)$ transition with a small contribution from $3d_{xy}(\pi)$ to $3d_{zz}(\sigma^*)$. The other two degenerate substates are regarded as the $3d_{xz}(\pi^*)$ to $3d_{yy}(\sigma^*)$ and the $3d_{yz}(\pi^*)$ to $3d_{xx}(\sigma^*)$ transitions. Here, we have used another set of nonorthogonal MOs $\{3d_{zz}(\sigma^*), 3d_{xx}(\sigma^*), \text{ and } 3d_{yy}(\sigma^*)\}$ from $\{3d_{zz}(\sigma^*) \text{ and } 3d_{xx-yy}(\sigma^*)\}$, which was obtained from the following relationships:

$$3d_{xx-yy} + 2d_{zz-(xx+yy)}/2 = -4d_{yy-(xx+zz)}/2 \quad (12)$$

$$3d_{xx-yy} - 2d_{zz-(xx+yy)}/2 = 4d_{xx-(yy+zz)}/2 \quad (13)$$

While the solvent effect in the results of the 1D-RISM-SCF method showed a large blue shift for both states, the 3D-RISM-SCF method showed a small red shift for the first state and a blue shift for the second state. The solvent effect on the excitation energy in the results of the 3D-RISM-SCF method was small, but the solvent effect had the tendency to improve the DFT results. These two states with dominant d–d transitions should have a small contribution from the second or third shell solvent molecules. We find the 3D-RISM-SCF method to agree with the above chemical intuition, while the 1D-RISM-SCF method seems to somewhat overestimate the shift.

The excitation energy to the third state (3^4T) with the DFT, 3D-RISM-SCF, and 1D-RISM-SCF methods was 5.60, 5.62, and 6.11 eV, respectively. The 1D-RISM-SCF energy is rather high compared with the other two methods. However, the orbital pictures are not so different. This is probably because these states have a large contribution from the ligand-to-metal

charge-transfer (LMCT) excitation, as is clearly indicated by lp_y to $3d_{zz}(\sigma^*)$ in the initial substate. The two other degenerate substates can be rewritten as lp_x to $3d_{yy}(\sigma^*)$ and lp_z to $3d_{xx}(\sigma^*)$ using eqs 12 and 13, as in the case of the 2^4T states.

The fourth state (4^4T) can be regarded as an LMCT excited state. The computed energies are 5.81, 5.80, and 6.24 eV. The orbital pictures are lp_y to $3d_{xx-yy}(\sigma^*)$, lp_x to $3d_{xx-zz}(\sigma^*)$, and lp_z to $3d_{yy-zz}(\sigma^*)$, where we have used eqs 10 and 11.

While the solvent effect in the results of the 1D-RISM-SCF method showed a large blue shift for both states, the 3D-RISM-SCF method showed a small blue shift for the third state and a red shift for the fourth state. The solvent effect on the excitation energy in the results of the 3D-RISM-SCF method was again very small. These two states with LMCT transitions should have larger contributions from the second or third shell of solvent molecules than the first two states because ligand water molecules have a direct interaction with the water molecules of the outer solvent shells. Both the 1D-RISM-SCF and 3D-RISM-SCF methods agree with the above chemical intuition.

Overall, the gas phase DFT and 3D-RISM-SCF methods gave close results, whereas the 1D-RISM-SCF methods overestimated the excitation energies. The source of the difference is the difference in the geometry, especially the bond distance between Cr and O. In fact, we carried out the 1D-RISM-SCF calculation at the 3D-RISM-SCF geometry and obtained similar results to the 3D-RISM-SCF method. The excitation energies obtained in such a way are 2.24 (1^4T), 2.89 (2^4T), 5.72 (3^4T), and 5.90 eV (4^4T), which are closer to the 3D-RISM-SCF results than the 1D-RISM-SCF results at the 1D-RISM-SCF optimized geometry. The small increase in the 3^4T and 4^4T states energies is probably due to the difference in orbital energy splittings.

IV. CONCLUSIONS

We examined the electronic structures of $[\text{Cr}(\text{H}_2\text{O})_6]^{3+}$ in aqueous solution as an example of transition metal ions in solution, using 3D- and 1D-RISM-SCF methods. The obtained geometries showed T_h and T symmetry in the gas and solution phases, respectively. The geometry obtained with the gas phase DFT and 3D-RISM-SCF methods were very similar except for the difference of T_h and T symmetry, while that obtained with the 1D-RISM-SCF method gave a somewhat smaller Cr–O bond length, which can be attributed to the larger polarization of the Cr and O atoms coming from the overestimation of the electrostatic interaction in 1D-RISM. The 3D distribution around $[\text{Cr}(\text{H}_2\text{O})_6]^{3+}$, which was determined with the 3D-RISM-SCF method simultaneously with the geometry and electronic structure of the solute, showed 12 maximum density points due to hydrogen bonds, as well as eight local maximum points at the hollow sites, in the second hydration shell. The 3D distribution function also showed 20 local maximum sites in the third hydration shell. The radial distribution functions obtained by angular averaging were consistent with the functions obtained using the 1D-RISM-SCF method. The low-lying excited states of vertical transitions were computed by the TD-DFT method including the electric field obtained by the 3D- and 1D-RISM-SCF methods. The electronic configurations and excitation energies obtained using DFT and 3D-RISM-SCF were very similar, although the orbital energies involved in the transition were rather different. The two lowest excited states were roughly assigned to the d–d transitions and the third and fourth excited states were assigned

to the LMCT transitions. The computed transition energies are in good agreement with the experimental values. In contrast, the excitation energies obtained using the 1D-RISM-SCF method were a little larger, probably because of the shorter Cr–O distances. The orbital shapes in the gas and solution phases were similar, and thus, the destabilization in orbital energies was nearly uniform, which is a reason for the similar transition energies. The difference comes not from the electronic structure, but from the geometry difference. These facts imply that the cluster model $[M(H_2O)_6]^{2+,3+}$ (namely, a model without solvent molecules beyond the first hydration shell) can be a good model for studying low-lying states if the effect of the solvent on the geometry is small.

AUTHOR INFORMATION

Corresponding Author

*E-mail: noriwo@chem.kyushu-univ.jp (N.Y.); nakano@chem.kyushu-univ.jp (H.N.).

Present Address

†(Y.K.) RIKEN Advanced Institute for Computational Science, 7-1-26, Minatojima-minami-machi, Chuo-ku, Kobe 650-0047, Japan.

Notes

The authors declare no competing financial interest.

ACKNOWLEDGMENTS

This work was partially supported by a Grant-in-Aid for Scientific Research (Nos. 23550018 and 24655018) from the Ministry of Education, Culture, Sports, Science and Technology in Japan.

REFERENCES

- (1) Aakesson, R.; Pettersson, L. G. M.; Sandstroem, M.; Siegbahn, P. E. M.; Wahlgren, U. Theoretical ab Initio SCF Study of Binding Energies and Ligand-Field Effects for the Hexahydrated Divalent Ions of the First-Row Transition Metals. *J. Phys. Chem.* **1992**, *96*, 10773–10779.
- (2) Landry-Hum, J.; Bussière, G.; Daniel, C.; Reber, C. Triplet Electronic States in d^2 and d^8 Complexes Probed by Absorption Spectroscopy: A CASSCF/CASPT2 Analysis of $[V(H_2O)_6]^{3+}$ and $[Ni(H_2O)_6]^{2+}$. *Inorg. Chem.* **2001**, *40*, 2595–2601.
- (3) (a) D'Angelo, P.; Barone, V.; Chillemi, G.; Sanna, N.; Meyer-Klaucke, W.; Pavel, N. V. Hydrogen and Higher Shell Contributions in Zn^{2+} , Ni^{2+} , and Co^{2+} Aqueous Solutions: An X-ray Absorption Fine Structure and Molecular Dynamics Study. *J. Am. Chem. Soc.* **2002**, *124*, 1958–1967. (b) Chillemi, G.; D'Angelo, P.; Pavel, N. V.; Sanna, N.; Barone, V. Development and Validation of an Integrated Computational Approach for the Study of Ionic Species in Solution by Means of Effective Two-Body Potentials. *J. Am. Chem. Soc.* **2002**, *124*, 1968–1976.
- (4) (a) Marini, G. W.; Liedl, K. R.; Rode, B. M. Investigation of Cu^{2+} Hydration and the Jahn–Teller Effect in Solution by QM/MM Monte Carlo Simulations. *J. Phys. Chem. A* **1999**, *103*, 11387–11393. (b) Pranowo, H. D.; Rode, B. M. Simulation of Preferential Cu^{2+} Solvation in Aqueous Ammonia Solution by Means of Monte Carlo Method Including Three-Body Correction Terms. *J. Chem. Phys.* **2000**, *112*, 4212. (c) Inada, Y.; Mohammed, A. M.; Loeffler, H. H.; Rode, B. M. Hydration Structure and Water Exchange Reaction of Nickel (II) Ion: Classical and QM/MM Simulations. *J. Phys. Chem. A* **2002**, *106*, 6783–6791.
- (5) (a) Iuchi, S.; Morita, A.; Kato, S. Potential Energy Surfaces and Dynamics of Ni^{2+} Ion Aqueous Solution: Molecular Dynamics Simulation of the Electronic Absorption Spectrum. *J. Chem. Phys.* **2004**, *121*, 8446–8457. (b) Iuchi, S.; Sakaki, S. Spin–Orbit Coupling in a Model Hamiltonian for d–d Excited States of Ni^{2+} Ion Aqueous Solution. *Chem. Phys. Lett.* **2010**, *485*, 114–118.
- (6) Kovalenko, A.; Hirata, F. Self-Consistent Description of a Metal–Water Interface by the Kohn–Sham Density Functional Theory and the Three-Dimensional Reference Interaction Site Model. *J. Chem. Phys.* **1999**, *110*, 10095–10112.
- (7) Sato, H.; Kovalenko, A.; Hirata, F. Self-Consistent Field, Ab Initio Molecular Orbital and Three-Dimensional Reference Interaction Site Model Study for Solvation Effect on Carbon Monoxide in Aqueous Solution. *J. Chem. Phys.* **2000**, *112*, 9463–9468.
- (8) (a) Ten-no, S.; Hirata, F.; Kato, S. A Hybrid Approach for the Solvent Effect on the Electronic Structure of a Solute Based on the RISM and Hartree–Fock Equations. *Chem. Phys. Lett.* **1993**, *214*, 391–396. (b) Ten-no, S.; Hirata, F.; Kato, S. Reference Interaction Site Model Self-Consistent Field Study for Solvation Effect on Carbonyl Compounds in Aqueous Solution. *J. Chem. Phys.* **1994**, *100*, 7443–7453. (c) Sato, H.; Hirata, F.; Kato, S. Analytical Energy Gradient for the Reference Interaction Site Model Multiconfigurational Self-Consistent-Field Method: Application to 1,2-Difluoroethylene in Aqueous Solution. *J. Chem. Phys.* **1996**, *105*, 1546–1551.
- (9) Kovalenko, A.; Hirata, F. Three-Dimensional Density Profiles of Water in Contact with a Solute of Arbitrary Shape: a RISM Approach. *Chem. Phys. Lett.* **1998**, *290*, 237–244.
- (10) Beglov, D.; Roux, B. An Integral Equation To Describe the Solvation of Polar Molecules in Liquid Water. *J. Phys. Chem. B* **1997**, *101*, 7821–7826.
- (11) (a) Chandler, D.; Andersen, H. C. Optimized Cluster Expansions for Classical Fluids. II. Theory of Molecular Liquids. *J. Chem. Phys.* **1972**, *57*, 1930–1937. (b) Hirata, F.; Rossky, P. J. An Extended RISM Equation for Molecular Polar Fluids. *Chem. Phys. Lett.* **1981**, *83*, 329–334.
- (12) (a) Gusarov, S.; Ziegler, T.; Kovalenko, A. Self-Consistent Combination of the Three-Dimensional RISM Theory of Molecular Solvation with Analytical Gradients and the Amsterdam Density Functional Package. *J. Phys. Chem. A* **2006**, *110*, 6083–6090. (b) Yoshida, N.; Hirata, F. A New Method to Determine Electrostatic Potential around a Macromolecule in Solution from Molecular Wave Functions. *J. Comput. Chem.* **2006**, *27*, 453–462.
- (13) (a) Becke, A. D. Density-Functional Thermochemistry. III. The Role of Exact Exchange. *J. Chem. Phys.* **1993**, *98*, 5648–5652. (b) Lee, C.; Yang, W.; Parr, R. G. Development of the Colle–Salvetti Correlation-Energy Formula into a Functional of the Electron Density. *Phys. Rev. B* **1988**, *37*, 785–789.
- (14) (a) Dunning, T. H. Gaussian Basis Sets for Use in Correlated Molecular Calculations. I. The Atoms Boron through Neon and Hydrogen. *J. Chem. Phys.* **1989**, *90*, 1007–1023. (b) Balabanov, N. B.; Peterson, K. A. Systematically Convergent Basis Sets for Transition Metals. I. All-Electron Correlation Consistent Basis Sets for the 3d Elements Sc–Zn. *J. Chem. Phys.* **2005**, *123*, 64107.
- (15) (a) Barysz, M.; Sadlej, A. J. Infinite-Order Two-Component Theory for Relativistic Quantum Chemistry. *J. Chem. Phys.* **2002**, *116*, 2696–2704. (b) Kędziera, D.; Barysz, M.; Sadlej, A. J. Expectation Values in Spin-Averaged Douglas–Kroll and Infinite-Order Relativistic Methods. *Struct. Chem.* **2004**, *15*, 369–377. (c) Kędziera, D.; Barysz, M. Two-Component Relativistic Methods for the Heaviest Elements. *J. Chem. Phys.* **2004**, *121*, 6719–6727. (d) Barysz, M.; Mentel, Ł.; Leszczyński, J. Recovering Four-Component Solutions by the Inverse Transformation of the Infinite-Order Two-Component Wave Functions. *J. Chem. Phys.* **2009**, *130*, 164114.
- (16) Berendsen, H. J. C.; Grigera, J. R.; Straatsma, T. P. The Missing Term in Effective Pair Potentials. *J. Phys. Chem.* **1987**, *91*, 6269–6271.
- (17) Hoops, S. C.; Anderson, K. W.; Merz, M., Jr. Force Field Design for Metalloproteins. *J. Am. Chem. Soc.* **1991**, *113*, 8262–8270.
- (18) Schmidt, M. W.; Baldrige, K. K.; Boatz, J. A.; Elbert, S. T.; Gordon, M. S.; Jensen, J. H.; Koseki, S.; Matsunaga, N.; Nguyen, K. A.; Su, S.; et al. General Atomic and Molecular Electronic Structure System. *J. Comput. Chem.* **1993**, *14*, 1347–1363.
- (19) Bleuzen, A.; Foglia, F.; Furet, E.; Helm, L.; Merbach, A. E.; Weber, J. Second Coordination Shell Water Exchange Rate and

Mechanism: Experiments and Modeling on Hexaaquachromium (III). *J. Am. Chem. Soc.* **1996**, *118*, 12777–12787 and references therein.

(20) Pappalardo, R. R.; Martínez, J. M.; Marcos, E. S. Application of the Hydrated Ion Concept for Modeling Aqueous Solutions Containing Highly Charged Ions: A Monte Carlo Simulation of Cr^{3+} in Water Using an ab Initio Intermolecular Potential. *J. Phys. Chem.* **1996**, *100*, 11748–11754.

(21) Figgis, B. N. *Introduction to Ligand Fields*; Interscience Publishers: New York, 1966.